THE JOURNAL OF PHYSICAL CHEMISTRY B

Article

pubs.acs.org/JPCB

Thermodynamic Investigation of the Effect of Interface Curvature on the Solid−Liquid Equilibrium and Eutectic Point of Binary Mixtures

Fanghui Liu, Leila Zargarzadeh, Hyun-Joong Chung, and Janet A. W. Elliott*

Department of Chemical and Materials Engineering, University of Alberta, Edmonton, Alberta, Canada T6G 1H9

ABSTRACT: Thermodynamic phase behavior is affected by curved interfaces in micro- and nanoscale systems. For example, capillary freezing point depression is associated with the pressure difference between the solid and liquid phases caused by interface curvature. In this study, the thermal, mechanical, and chemical equilibrium conditions are derived for binary solid−liquid equilibrium with a curved solid−liquid interface due to confinement in a capillary. This derivation shows the equivalence of the most general forms of the Gibbs−Thomson and Ostwald−Freundlich equations. As an example, the effect of curvature on solid−liquid equilibrium is explained quantitatively for the water/glycerol system. Considering the effect of a curved solid−liquid interface, a complete solid−liquid phase diagram is developed over a range of concentrations for the water/glycerol system (including the freezing of pure water or precipitation of pure glycerol depending on the concentration of the solution). This phase diagram is compared with the traditional phase diagram in which the assumption of a flat solid−liquid interface is made. We show the extent to which nanoscale interface curvature can affect the composition-dependent freezing and precipitating processes, as well as the change in the eutectic point temperature and concentration with interface curvature. Understanding the effect of curvature on solid−liquid equilibrium in nanoscale capillaries has applications in the food industry, soil science, cryobiology, nanoporous materials, and various nanoscience fields.

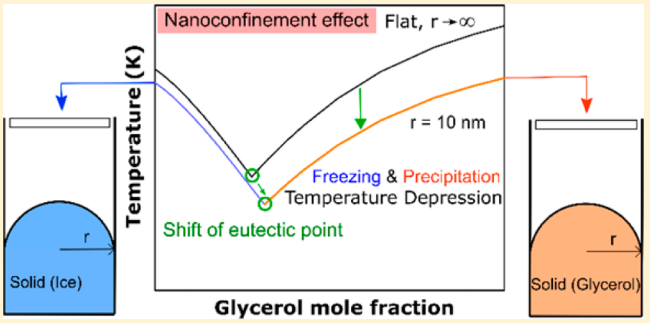

1. INTRODUCTION

1.1. Effect of Phase Boundary Curvature on Phase Diagrams. Understanding the fundamental science of solid, liquid, or vapor confined in capillaries or pores is significant in surface chemistry and physics. Different equations have been proposed to explain the effect of phase boundary curvature on equilibrium. One of the most well-known equations is the Kelvin equation that describes the equilibrium vapor pressure above a curved interface compared to the vapor pressure above a flat interface at the same temperature. The initial equation derived by Lord Kelvin[1] was only approximate. It was not thermodynamically correct as it did not consider chemical potential equilibrium.[2] In the corrected form of the Kelvin equation, the mechanical equilibrium (Laplace equation) is combined with the chemical potential equilibrium.[3,4] The Kelvin equation can be applied to drops, bubbles, and capillary-held wetting liquid menisci, and it has been validated for surfaces with mean radii of curvature larger than 8 times the molecular diameter of the material of interest (for example, for cyclohexane, the Kelvin equation is valid down to a radius of curvature of 4 nm).[5,6] Later on, several groups extended the Kelvin equation to multicomponent mixtures in vapor−liquid equilibrium,[7,8] taking into account the chemical potential equilibrium for multiple components in different phases, that is, the equality of the chemical potential of each component in different phases.[9] Although the Kelvin equation was initially derived for the case of vapor−liquid equilibrium, the idea can be extended to liquid−liquid equilibrium. The liquid−liquid analogue of the Kelvin equation has been applied to investigate the thermodynamic equilibrium of micro- and nanodrops concentrated by partial dissolution into a surrounding oil phase.[10,11]

The Gibbs−Thompson equation is an analogue of the Kelvin equation for solid−liquid equilibrium that describes the equilibrium melting point of a small pure solid crystal in its own pure liquid as a function of crystal radius. The validity of the Gibbs−Thompson equation has been proven by experiments.[12,13] There are many experiments showing the effect of curvature on phase equilibrium in a range of porous systems: metal oxide gels, porous glasses, and nanoporous materials.[14] For single-component solid−liquid equilibrium confined inside of pores, the experimental results have been compared with theoretical predictions to show the relevance of the size of the pores.[15,16] The capillary freezing point inside of glass capillaries with radii of 3−87 μm was measured while the image of the ice−solution interface was captured to analyze the contact angle.[13] For porous materials with different nanoscale curvature in single-component solid−liquid equilibrium, the freezing temperature of liquid in a pore is lower than that of bulk liquid with a flat surface. The Gibbs−Thompson equation has been shown to be valid to predict the freezing and melting point depression of ice in nanoscopic glass pores that are as small as

Received: July 23, 2017
Revised: August 30, 2017
Published: September 29, 2017

DOI: 10.1021/acs.jpcb.7b07271
J. Phys. Chem. B 2017, 121, 9452−9462

~4 nm in diameter.[17] The Gibbs–Thompson equation can also be extended for multicomponent systems in solid–liquid equilibrium. In cryobiology, in which cells in solution or tissues are subjected to low temperatures, the temperature at which ice propagates through confined spaces is lowered by the Gibbs–Thomson effect.[18−20] Also, the Gibbs–Thomson equation has been applied to predict microstructure formation during solidification in multicomponent systems.[21]

The Ostwald–Freundlich equation is another analogue of the Kelvin equation for solid–liquid equilibrium. Introduced by Ostwald[22] and later corrected by Freundlich,[23] the Ostwald–Freundlich equation[24] expresses the solubility of a solid particle in a bulk liquid solution as a function of particle curvature. As the size of the solids is decreased to the nanoscale, the solubility will depend on the size of the particle.[25] A nonideal form of the Ostwald–Freundlich equation developed by Eslami et al. was used to describe the effect of precipitate solute curvature on aqueous microdrop concentrating processes.[26]

The references mentioned above consider only the computation of the equilibrium state in a narrow range of concentrations. Studies of the effect of curvature on phase equilibrium in multicomponent systems have been quite limited compared with those of single-component systems. To our knowledge, a rigorous thermodynamic study has not been done of the effects of curvature on solid–liquid equilibrium in multicomponent systems over the complete range of concentrations and temperatures.

Some recent works studied the effect of curvature on multicomponent vapor–liquid equilibrium.[27,28] In nanosized pores in which vapor and liquid phases coexist, equation-of-state models have been used to describe capillary condensation for binary mixtures and to calculate the critical pore radius and condensed-phase equilibrium pressure for nanosized pores.[27,29] Another example by Shardt and Elliott is the investigation of the curvature effect on multicomponent vapor–liquid phase equilibrium. They developed phase envelopes and phase composition diagrams for the ideal system methanol/ethanol and the nonideal system ethanol/water. They showed that the azeotrope (equal volatility point in nonideal systems) shifts with nanoscale curvature.[28]

In the field of materials science, several studies attempted to model phase diagrams for nanoscale alloys by adding surface thermodynamic terms to the Gibbs free energy of bulk available in CALPHAD (CALculation of PHAse Diagram).[30,31] However, that approach is not consistent with the Gibbsian thermodynamics of composite systems,[2] which is the basis of the work presented here. That approach[30,31] does not lead to the well-known Gibbs–Thomson equation and Ostwald–Freundlich equations.

In this work, we develop the effect of solid curvature on the solid–liquid phase diagram across the entire composition range for any arbitrary binary solution that forms pure solids including the effect of the contact angle at which the solid–liquid interface contacts a confining pore wall.

1.2. Solid–Liquid Phase Diagrams in the Absence of Curvature. Solid–liquid phase diagrams can have many complexities. However, there are many multicomponent systems for which the solid phases are in pure form because of the differences in molecular size and/or molecular structure.[32] Partial miscibility of solid phases (resulting in nonpure solid phases) is uncommon in cases other than metallic systems.[33] Here, our focus is on aqueous solutions. For the purposes of this paper, we restrict our discussion to binary systems in which a pure solid phase is in equilibrium with a solution. Such systems have only two possible solid phases and a single eutectic point.

An illustrative phase diagram in Figure 1 describes the phase behavior of such a two-component mixture at constant pressure. At higher temperature, the solution exists as a single phase, that is, an unsaturated stable homogeneous liquid phase. At lower temperature, the liquid separates into a *pure* solid phase and a liquid solution. The component of the pure solid phase depends on the concentration of the liquid solution. If we choose one component to call the solvent and one to call the solute, the left part of Figure 1 is the freezing process of the solvent and the right part is the precipitating process of the solute.

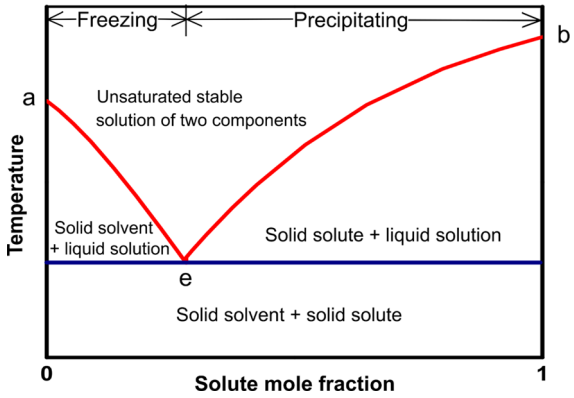

Figure 1. Illustrative constant pressure, temperature–composition phase diagram of solid–liquid equilibrium in a binary system with a simple eutectic and pure solid phases above the eutectic temperature.

Liquidus lines (curves ae and be) in Figure 1 represent the onset of solidification. In the case of an aqueous solution, curve ae shows the composition-dependent freezing point depression, whereas curve eb represents the concentration-dependent solubility limit of the other component in the aqueous solution. The liquidus lines also show the concentration of the unfrozen or unprecipitated solution at a given temperature. The left and right liquidus meet at a minimum point e, called the eutectic ("easy melting") point.[33] The eutectic point is the point where solid solute, solid solvent, and liquid mixture coexist. The eutectic point is the lowest temperature for the given pressure at which the liquid phase is stable. Below the eutectic point, the system consists of two pure solid phases. When a liquid solution of a given overall composition is cooled, the system temperature lowers at constant composition until a liquidus line is met and solidification begins, and with further cooling, the composition of the remaining liquid follows the liquidus line to the eutectic point.

1.3. Objectives of this Work. The phase diagram shown in Figure 1 is constructed under the assumption that the interface between the solid and liquid is flat. In this paper, we apply Gibbsian composite system thermodynamics to understand the effect of interface curvature on solid–liquid phase equilibrium in a binary mixture. We start by deriving the general conditions for solid–liquid equilibrium in a capillary that imposes a curved solid–liquid interface. The conditions for equilibrium are then examined for the case of the water/glycerol system, quantifying the effect of interface curvature on the two liquidus lines (freezing point temperature as a function of concentration and precipitation saturation concentration as a function of temper-

DOI: 10.1021/acs.jpcb.7b07271
J. Phys. Chem. B 2017, 121, 9452−9462

ature). The eutectic point temperature and concentration are also calculated. As an example to explore the effects of curvature, we chose the water/glycerol binary system because this system exhibits complete miscibility in the liquid state and nearly complete insolubility between components in the respective solid states (i.e., pure component solids). Furthermore, water/glycerol solid−liquid phase diagrams have important applications because glycerol is a popular antifreeze substance, the first permanent type antifreeze agent for radiator cooling systems in automobiles,[34] and the first cryoprotectant for preserving living cells.[35]

2. GOVERNING EQUATIONS

2.1. Derivation of General Conditions for Solid−Liquid Equilibrium and Calculating the Liquidus Lines (Freezing and Solute Precipitation) and Eutectic Point.

Gibbsian thermodynamics of composite systems gives a formal approach for finding the conditions for equilibrium of a multiphase multicomponent system by extremizing entropy subject to constraints on the system. Our objective is to find the effect of confinement in a capillary of radius r on the solid−liquid phase diagram of a two-component aqueous system. Here, the largest radius of curvature that a solid phase forming out of the aqueous solution can have is defined by the interaction with the capillary wall. Thus, we consider the equilibrium of the system illustrated in Figure 2, where a single-component solid phase is in equilibrium with a two-component liquid phase and where the curved solid−liquid interface contacts the capillary wall at the contact angle, θ.

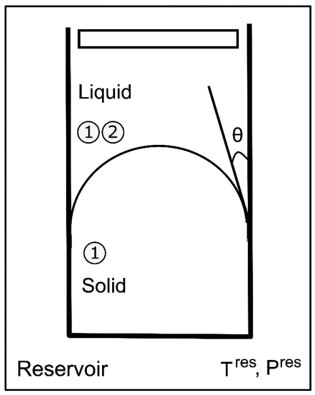

Figure 2. Schematic of solid−liquid equilibrium with a curved solid−liquid interface in a capillary.

We assign the solid components in the capillary wall to be part of the reservoir and assign the liquid−capillary and solid−capillary interfaces to be parts of the system.[2] The solid phase can be either pure ice or pure precipitated solute as we limit our study to only those aqueous solutions in which ice forms as pure water or solute precipitates as pure solute. Component 1 represents the molecules that are in the solid phase and liquid phase, and component 2 represents the other molecules that are in the liquid phase. The solid−liquid interface contains molecules of both components 1 and 2. The liquid−capillary and solid−capillary interfaces are considered to be part of the system so that adsorption of components 1 and 2 at the liquid−capillary and solid−capillary interfaces is included in consideration. The pressure and temperature of the reservoir surrounding the system (including the capillary solid), P^{res} and T^{res}, respectively, are considered to remain constant. The system does not exchange any mass with the reservoir; therefore, the number of molecules of each component in the system is constant. Molecules of component 1 are present in the solid phase (solid solvent or precipitate), the liquid phase (solvent/solute mixture), the solid−liquid interface, the liquid−capillary interface, and the solid−capillary interface. Molecules of component 2 are present in the liquid phase, the solid−liquid interface, and the liquid−capillary interface; however, they do not exist in the solid or the solid−capillary interface.

We can find the conditions for equilibrium of the system by finding the conditions that extremize entropy of the system plus reservoir

$$dS = dS^{S} + dS^{L} + dS^{SC} + dS^{LC} + dS^{SL} + dS^{res} = 0 \tag{1}$$

where S^S, S^L, and S^{res} are the entropies of the solid phase, the liquid phase, and the reservoir and S^{SC}, S^{LC}, S^{SL} are the entropies of the solid−capillary, liquid−capillary, and solid−liquid interfaces, respectively. The entropy differentials can be written as in eqs 2−7 using the fundamental relations and the definitions of intensive properties temperature T, pressure P, and chemical potential μ.[36] The differential of entropy of the liquid phase (superscript L) is written as

$$dS^{L} = \frac{1}{T^{L}}dU^{L} + \frac{P^{L}}{T^{L}}dV^{L} - \frac{\mu_1^{L}}{T^{L}}dN_1^{L} - \frac{\mu_2^{L}}{T^{L}}dN_2^{L} \tag{2}$$

where V is volume, U is internal energy, μ_i^L is the chemical potential of component i in the liquid phase, and N_i^L is the number of moles of component i in the liquid phase. Because component 2 does not exist in the solid phase, the differential of entropy of the solid phase (superscript S) is written as

$$dS^{S} = \frac{1}{T^{S}}dU^{S} + \frac{P^{S}}{T^{S}}dV^{S} - \frac{\mu_1^{S}}{T^{S}}dN_1^{S} \tag{3}$$

Using the Gibbs Surface of Tension approach, the curved solid−liquid interface (superscript SL) is treated as a phase that has area but no volume and to which are assigned excess properties (S^{SL}, U^{SL}, N_1^{SL}, N_2^{SL}) and an interfacial tension σ, the value for which does not depend explicitly on curvature. Therefore, the differential of the solid−liquid interface entropy is given by

$$dS^{SL} = \frac{1}{T^{SL}}dU^{SL} - \frac{\sigma^{SL}}{T^{SL}}dA^{SL} - \frac{\mu_1^{SL}}{T^{SL}}dN_1^{SL} - \frac{\mu_2^{SL}}{T^{SL}}dN_2^{SL} \tag{4}$$

where A is the area of the interface, μ_1^{SL} represents the chemical potential of surface excess component 1 molecules, and σ^{SL} represents the solid−liquid interfacial tension.

Because the radius of the capillary will not be changing as the system evolves to equilibrium, it is convenient to adopt the Gibbs Dividing Surface approach in which the dividing surfaces between the capillary and either the liquid or solid phases are placed such that there are no excess moles of the capillary solid material in the interfaces. We will be either leaving the contact angle as a variable or setting the contact angle; hence, we will not have to explicitly introduce any curvature dependence for the interfacial tension of the capillary solid and therefore proceed without loss of generality. This is also consistent with defining the reservoir to contain all molecules of the capillary solid. Therefore, the differential of the entropy of the liquid−capillary interface (superscript LC) is

DOI: 10.1021/acs.jpcb.7b07271
J. Phys. Chem. B 2017, 121, 9452−9462

$$dS^{LC} = \frac{1}{T^{LC}}dU^{LC} - \frac{\sigma^{LC}}{T^{LC}}dA^{LC} - \frac{\mu_1^{LC}}{T^{LC}}dN_1^{LC} - \frac{\mu_2^{LC}}{T^{LC}}dN_2^{LC} \quad (5)$$

and the differential of the entropy of the solid−capillary interface (superscript SC) is

$$dS^{SC} = \frac{1}{T^{SC}}dU^{SC} - \frac{\sigma^{SC}}{T^{SC}}dA^{SC} - \frac{\mu_1^{SC}}{T^{SC}}dN_1^{SC} \quad (6)$$

Finally, the differential of the entropy of the reservoir (superscript res) may be written

$$dS^{res} = \frac{1}{T^{res}}dU^{res} + \frac{P^{res}}{T^{res}}dV^{res} - \frac{\mu^{res}}{T^{res}}dN^{res} \quad (7)$$

Next the system constraints are enumerated. The total internal energy of the system plus reservoir is constant

$$dU^{res} = -dU^{S} - dU^{L} - dU^{SL} - dU^{SC} - dU^{LC} \quad (8)$$

The total volume of the system plus reservoir is constant

$$dV^{res} = -dV^{S} - dV^{L} \quad (9)$$

The total number of moles of component 1 in the system (solid phase, liquid phase, solid−liquid interface, solid−capillary interface, and liquid−capillary interface) is constant

$$dN_1^{S} = -dN_1^{L} - dN_1^{SL} - dN_1^{SC} - dN_1^{LC} \quad (10)$$

The total number of moles of component 2 in the system (liquid phase, liquid−capillary interface, and solid−liquid interface) is constant

$$dN_2^{L} = -dN_2^{SL} - dN_2^{LC} \quad (11)$$

The number of moles in the reservoir is also constant

$$dN^{res} = 0 \quad (12)$$

The next step is to use geometric knowledge to impose relationships between phase volumes and areas because changes in these are not independent. We assume that the solid−liquid interface takes the shape of a spherical cap with geometry as defined in Figure 3.

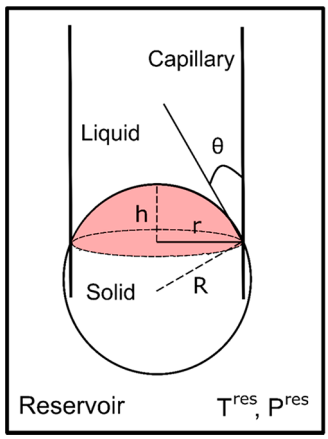

Figure 3. Schematic diagram of the geometry of solid−liquid equilibrium in a capillary. The solid−liquid interface is assumed to take the shape of a spherical cap with height h and base width equal to the capillary radius r. The radius of curvature of the solid−liquid interface is R.

Denoting the surface area of the spherical cap A_{cap}^{sph} and the volume of the spherical cap V_{cap}^{sph}, the following geometrical relationships are valid[37]

$$A_{cap}^{sph} = 2\pi Rh = \frac{2\pi r^2(1 - \sin\theta)}{\cos^2\theta} \quad (13)$$

$$V_{cap}^{sph} = \frac{\pi h(3r^2 + h^2)}{6} = \frac{\pi r^3(\sin^3\theta - 3\sin\theta + 2)}{3\cos^3\theta} \quad (14)$$

$$R = \frac{r}{\cos\theta} = \frac{h}{1 - \sin\theta} \quad (15)$$

The increase in the liquid−capillary area equals the decrease in the solid−capillary area

$$dA^{LC} = -dA^{SC} \quad (16)$$

The change in the area of the solid−liquid interface can be found by taking the derivative of eq 13

$$dA^{SL} = dA_{cap}^{sph} = \frac{4\pi r(1 - \sin\theta)}{\cos^2\theta}dr - \frac{2\pi r^2(\sin\theta - 1)^2}{\cos^3\theta}d\theta \quad (17)$$

The change in the volume of the solid can be found by realizing that the solid volume can be changed by changes in the volume of the spherical cap or by moving the spherical cap up or down in the capillary

$$\begin{aligned} dV^{S} &= dV_{cap}^{sph} + \frac{1}{2}r dA^{SC} \\ &= \frac{1}{2}r dA^{SC} + \frac{\pi r^2(2 - 3\sin\theta + \sin^3\theta)}{\cos^3\theta}dr \\ &\quad - \frac{\pi r^3(\sin\theta - 1)^2}{\cos^4\theta}d\theta \end{aligned} \quad (18)$$

Substituting eqs 2−7 into eq 1, making use of constraints in eqs 8−12 and 16−18, noting that because the temperature and pressure of the reservoir are fixed, $dr = 0$, and collecting like terms yields

$$\begin{aligned} &\left(\frac{1}{T^{L}} - \frac{1}{T^{res}}\right)dU^{L} + \left(\frac{1}{T^{S}} - \frac{1}{T^{res}}\right)dU^{S} + \left(\frac{1}{T^{SL}} - \frac{1}{T^{res}}\right)dU^{SL} \\ &+ \left(\frac{1}{T^{LC}} - \frac{1}{T^{res}}\right)dU^{LC} + \left(\frac{1}{T^{SC}} - \frac{1}{T^{res}}\right)dU^{SC} \\ &+ \left(\frac{\mu_1^{L}}{T^{L}} - \frac{\mu_1^{SC}}{T^{SC}}\right)dN_1^{L} + \left(\frac{\mu_1^{S}}{T^{S}} - \frac{\mu_1^{SC}}{T^{SC}}\right)dN_1^{S} \\ &+ \left(\frac{\mu_1^{SL}}{T^{SL}} - \frac{\mu_1^{SC}}{T^{SC}}\right)dN_1^{SL} + \left(\frac{\mu_1^{LC}}{T^{LC}} - \frac{\mu_1^{SC}}{T^{SC}}\right)dN_1^{LC} \\ &+ \left(\frac{\mu_2^{L}}{T^{L}} - \frac{\mu_2^{LC}}{T^{LC}}\right)dN_2^{L} + \left(\frac{\mu_2^{L}}{T^{SL}} - \frac{\mu_2^{LC}}{T^{LC}}\right)dN_2^{SL} \\ &+ \left(\frac{P^{L}}{T^{L}} - \frac{P^{res}}{T^{res}}\right)dV^{L} + \left[\frac{1}{2}r\left(\frac{P^{S}}{T^{S}} - \frac{P^{res}}{T^{res}}\right)\right. \\ &\left. + \left(\frac{\sigma^{LC}}{T^{LC}} - \frac{\sigma^{SC}}{T^{SC}}\right)\right]dA^{SC} + \left[\left(\frac{P^{S}}{T^{S}} - \frac{P^{res}}{T^{res}}\right)\right. \\ &\left.\left(\frac{-\pi r^3(\sin\theta - 1)^2}{\cos^4\theta}\right) - \frac{\gamma^{SL}}{T^{SL}}\left(\frac{-2\pi r^2(\sin\theta - 1)^2}{\cos^3\theta}\right)\right]d\theta = 0 \end{aligned} \quad (19)$$

DOI: 10.1021/acs.jpcb.7b07271
J. Phys. Chem. B 2017, 121, 9452−9462

After considering all constraints and geometrical relations, all differentials in eq 19 are independent. Therefore, for eq 19 to be true for any possible variation about equilibrium, the coefficients multiplying the differentials in eq 19 must each be set equal to zero, thus yielding the following conditions for equilibrium:

$$T^{S} = T^{L} = T^{SL} = T^{SC} = T^{LC} = T^{res} = T \tag{20}$$

$$\mu_1^{S} = \mu_1^{L} = \mu_1^{SL} = \mu_1^{SC} = \mu_1^{LC} \tag{21}$$

$$\mu_2^{L} = \mu_2^{SL} = \mu_2^{LC} \tag{22}$$

$$P^{L} = P^{res} \tag{23}$$

$$P^{S} - P^{L} = \frac{2\sigma^{SL}\cos\theta}{r} \tag{24}$$

$$\sigma^{SC} - \sigma^{LC} = \sigma^{SL}\cos\theta \tag{25}$$

Equation 20 is the thermal equilibrium condition. Equations 21 and 22 are chemical equilibrium conditions. Equation 23 is the mechanical equilibrium between the reservoir and liquid phase. Equations 24 and 25 are also mechanical equilibrium conditions; eq 24 is the Young–Laplace equation, and eq 25 is the Young equation.

By assuming that the system temperature T and the liquid-phase pressure P^{L} are set by the reservoir, the set of equilibrium conditions that arise from eqs 20–25 can be combined to calculate the liquidus lines. In eq 24, when the solid–liquid interface is flat, r goes to infinity and the pressure in the solid phase is equal to the pressure in the liquid phase. It should be noted that the radius of curvature is defined to be positive when the center of the circle that defines the interface is placed inside of the solid phase, that is, when the interface is curved toward the solid. We combine the thermal equilibrium (equality of temperature of the solid phase, liquid phase, and solid–liquid interface), the mechanical equilibrium of eqs 23 and 24, and the equality of the chemical potential of component 1 in the solid and liquid (the first equivalence in eq 21) to get

$$\mu_1^{L}(T, P^{L}, x_1^{L}) = \mu_1^{S}(T, P^{S}) \tag{26}$$

To develop the governing equation for the phase diagram, eq 24 and equations of state for the chemical potentials must be inserted into eq 26. The chemical potential of the solidifying component in the pure solid phase can be found by assuming that the solid phase is incompressible and that the solid molar entropy is independent of temperature and thus can be expressed by

$$\mu_1^{S}(T, P^{S}) = \mu_1^{S}(T_{m,1}, P^{L}) - s_1^{S}(T - T_{m,1}) + v_1^{S}(P^{S} - P^{L}) \tag{27}$$

where $T_{m,1}$, the melting point of pure component 1 at the pressure of the bulk phase (i.e., liquid-phase pressure P^{L}), is chosen as the reference point for calculating the chemical potential. s_1^{S} and v_1^{S} are the molar entropy and molar volume of pure component 1 in the solid phase at $T_{m,1}$ and P^{L}, respectively.

Before giving the chemical potential of component 1 in the liquid phase, we define auxiliary functions osmole fraction $\tilde{\pi}$, osmotic pressure Π, activity a, and activity coefficient γ by their relationships to the chemical potential in the liquid.[38−40]

$$\tilde{\pi} = -\frac{\mu_1^{L} - \mu_1^{L0}}{RT} \tag{28}$$

where μ_1^{L} is the chemical potential of component 1 in the liquid phase, μ_1^{L0} is the chemical potential of pure liquid component 1, and from here on, R is the universal gas constant. The activity of component 1 in solution can be expressed as

$$a_1^{L} = x_1^{L}\gamma_1^{L} \tag{29}$$

where a_1^{L} is the composition-dependent activity of component 1 in the binary solution and γ_1^{L} is the composition-dependent activity coefficient of component 1 in solution, which accounts for solution nonideality

$$\Pi = \frac{RT\tilde{\pi}}{v_1^{L}} = -\frac{RT\ln(a_1^{L})}{v_1^{L}} = -\frac{RT\ln(x_1^{L}\gamma_1^{L})}{v_1^{L}} \tag{30}$$

where v_1^{L} is the molar volume of pure liquid component 1 and Π is the binary solution composition-dependent osmotic pressure.

For the chemical potential of component 1 in the liquid solution, we use

$$\mu_1^{L}(T, P^{L}, x_1^{L}) = \mu_1^{L0}(T_{m,1}, P^{L}) - s_1^{L}(T - T_{m,1}) + RT\ln(x_1^{L}\gamma_1^{L}) \tag{31}$$

where s_1^{L} is the temperature-independent molar entropy of pure component 1 in liquid form at $T_{m,1}$ and P^{L}.

The chemical potential can equivalently be expressed in terms of osmotic pressure.[20]

$$\mu_1^{L}(T, P^{L}, x_1^{L}) = \mu_1^{L0}(T_{m,1}, P^{L}) - s_1^{L}(T - T_{m,1}) - v_1^{L}\Pi(T, x_1^{L}) \tag{32}$$

Substituting eqs 27 and 31 into eq 26, and replacing $(s_1^{L} - s_1^{S})$ using the thermodynamic identity

$$\frac{1}{s_1^{L} - s_1^{S}} = \frac{T_{m,1}}{\Delta H_1^{fus}} \tag{33}$$

where ΔH_1^{fus} is the molar enthalpy of fusion (latent heat of melting) for pure component 1 at $T_{m,1}$ and P^{L}, leads to

$$\ln(x_1^{L}\gamma_1^{L}) = \frac{\Delta H_1^{fus}}{RT_{m,1}}\left(1 - \frac{T_{m,1}}{T}\right) + \frac{v_1^{S}}{RT}(P^{S} - P^{L}) \tag{34}$$

Substituting the Laplace equation, eq 24, for the pressure difference term in eq 34 and rearranging for the solid–liquid equilibrium temperature yields

$$T = \frac{\frac{2v_1^{S}\sigma^{SL}\cos\theta}{r} - \Delta H_1^{fus}}{R\ln(x_1^{L}\gamma_1^{L}) - \frac{\Delta H_1^{fus}}{T_{m,1}}} \tag{35}$$

The freezing or precipitating temperature depression can be expressed as

$$T_{m,1} - T = \frac{RT_{m,1}\ln(x_1^{L}\gamma_1^{L}) - \frac{2v_1^{S}\sigma^{SL}\cos\theta}{r}}{R\ln(x_1^{L}\gamma_1^{L}) - \frac{\Delta H_1^{fus}}{T_{m,1}}} \tag{36}$$

Equation 36 is a very general form of both the Gibbs–Thomson equation and the Ostwald–Freundlich equation that also includes the effect of the contact angle. The way that we

DOI: 10.1021/acs.jpcb.7b07271
J. Phys. Chem. B 2017, 121, 9452−9462

have done this derivation highlights the equivalence of the Gibbs−Thomson and Ostwald−Freundlich equations. Equations 35 and 36 are each nonideal forms of both the Gibbs−Thomson equation and Ostwald−Freundlich equation, the naming of the equation depending only on which component is identified as component 1.

Alternatively and more commonly for the freezing process than the precipitating process, the solidifying point depression can also be written in terms of osmotic pressure

$$T_{m,1} - T = \frac{2\nu_1^S \sigma^{SL} T_{m,1} \cos\theta}{r\Delta H_1^{fus}\left(1 + \frac{RT_{m,1}\tilde{\pi}}{\Delta H_1^{fus}}\right)} + \frac{\frac{R\tilde{\pi}T_{m,1}^2}{\Delta H_1^{fus}}}{1 + \frac{R\tilde{\pi}T_{m,1}}{\Delta H_1^{fus}}}$$
$$= \frac{2\nu_1^S \sigma^{SL} T_{m,1} \cos\theta}{r\Delta H_1^{fus}} + \frac{\nu_1^L \Pi T_{m,1}}{\Delta H_1^{fus}} \quad (37)$$

The first term of eq 37 is the capillary effect, and the second term of eq 37 is the osmotic effect.[13] Equation 37 has an osmole fraction version and an osmotic pressure version. The osmotic pressure version can be found in previous work.[13,20] The second term of the osmole fraction version has been applied in multisolute nonideal solutions without curvature effects.[41]

For a flat solid−liquid interface, the pressure of the solid phase equals the pressure in the liquid phase and $\frac{2\nu_1^S\sigma^{SL}}{r}$ in eqs 35−37 is zero. For a curved interface, the pressure difference between the solid and liquid phases varies as a function of the radius of curvature according to eq 24, and the curvature term appears in eqs 35−37.

The freezing and precipitating liquidus lines meet at a minimum point, which is called the eutectic point. In order to calculate the eutectic point concentration and temperature, we use T_F and T_P to represent the freezing temperature of solvent and the precipitating temperature of solute, respectively. Then, according to eq 35 for the solidifying temperature and considering the fact that summation of the mole fractions in the liquid phase is 1 (hence, for a binary system $x^L_{solvent} + x^L_{solute} = 1$)

$$T_F = \frac{\frac{2\nu_F^S\sigma_F^{SL}\cos\theta_F}{r} - \Delta H_F^{fus}}{R\ln[(1 - x^L_{solute})\gamma_F^L] - \frac{\Delta H_F^{fus}}{T_{m,F}}} \quad (38)$$

$$T_P = \frac{\frac{2\nu_P^S\sigma_P^{SL}\cos\theta_P}{r} - \Delta H_P^{fus}}{R\ln(x^L_{solute}\gamma_P^L) - \frac{\Delta H_P^{fus}}{T_{m,P}}} \quad (39)$$

where x^L_{solute} is the mole fraction of solute in the liquid phase and v_F^S and v_P^S represent the molar volume of pure solvent solid phase in the freezing process and pure solute solid phase in the precipitating process, respectively. ΔH_F^{fus} and ΔH_P^{fus} represent the molar enthalpy of fusion of solvent in the freezing process and solute in the precipitating process. σ_F^{SL} and σ_P^{SL} represent the interfacial tensions of solid solvent−liquid solution in the freezing process and solid solute−liquid solution in the precipitating process, respectively. θ_F and θ_P represent the contact angle between the curved solid−liquid interface and the capillary in the freezing and precipitating process, respectively. γ_F^L and γ_P^L represent the activity coefficients of solvent in the liquid phase in the freezing process and solute in the liquid phase in the precipitating process, respectively. At the eutectic point, T_F equals T_P and equating eqs 38 and 39 yields an equation for the eutectic point solute concentration, x_E

$$\frac{\frac{2\nu_F^S\sigma_F^{SL}\cos\theta_F}{r} - \Delta H_F^{fus}}{R\ln[(1 - x_E)\gamma_F^L] - \frac{\Delta H_F^{fus}}{T_{m,F}}} = \frac{\frac{2\nu_P^S\sigma_P^{SL}\cos\theta_P}{r} - \Delta H_P^{fus}}{R\ln(x_E\gamma_P^L) - \frac{\Delta H_P^{fus}}{T_{m,P}}} \quad (40)$$

which can be solved together with eq 35 for the eutectic temperature. It has already been noted in previous work that the eutectic point concentration equation for a binary system with a flat surface is usually a transcendental equation,[42] which is difficult to solve directly. Therefore, linear fitting[43] and polynomial fitting[44] are used. Here, we give the transcendental equation for the eutectic solute concentration in the case of curved interfaces. Equation 40 can be solved numerically together with eq 35 to yield the eutectic solute concentration and the eutectic temperature for a given curvature.

In order to present the maximum effect of curvature and for lack of the required information to do otherwise, we take the contact angle that either the ice−liquid interface or the glycerol precipitate−liquid interface makes with the capillary solid wall to be zero for this exploration. Note that this is also equivalent to considering a nucleating sphere of either ice or precipitate without interaction with the capillary solid, the maximum radius of curvature of which equals the radius of the capillary. By setting the contact angle equal to zero, we have removed from our concern the role of adsorption at the capillary solid wall. For this work, the zero contact angle assumption may exaggerate the predicted freezing/precipitation point depression due to the capillary radius. In the case of zero contact angle, eq 35 becomes

$$T = \frac{\frac{2\nu_1^S\sigma^{SL}}{r} - \Delta H_1^{fus}}{R\ln(x_1^L\gamma_1^L) - \frac{\Delta H_1^{fus}}{T_{m,1}}} \quad (41)$$

The freezing or precipitating temperature depression can be expressed as

$$T_{m,1} - T = \frac{RT_{m,1}\ln(x_1^L\gamma_1^L) - \frac{2\nu_1^S\sigma^{SL}}{r}}{R\ln(x_1^L\gamma_1^L) - \frac{\Delta H_1^{fus}}{T_{m,1}}} \quad (42)$$

The eutectic concentration is then given by

$$\frac{\frac{2\nu_F^S\sigma_F^{SL}}{r} - \Delta H_F^{fus}}{R\ln[(1 - x_E)\gamma_F^L] - \frac{\Delta H_F^{fus}}{T_{m,F}}} = \frac{\frac{2\nu_P^S\sigma_P^{SL}}{r} - \Delta H_P^{fus}}{R\ln(x_E\gamma_P^L) - \frac{\Delta H_P^{fus}}{T_{m,P}}} \quad (43)$$

2.2. Freezing and Precipitation Liquidus Line and Eutectic Point Calculation for the Water/Glycerol System. After finding the general form of the conditions for solid−liquid equilibrium, the next step is to solve this set of equations for the system of interest in this article, which is the water/glycerol system. We want to compute the liquidus lines of the phase diagram, that is, the freezing point as a function of composition (solidification of solvent water) and the precipitation saturation composition as a function of temperature (solidification of solute glycerol). We wish to compare such a phase diagram computed in the presence of a curved solid−liquid interface (i.e., confined in a capillary) to the traditional phase diagram computed for a flat solid−liquid interface (unconfined).

DOI: 10.1021/acs.jpcb.7b07271
J. Phys. Chem. B 2017, 121, 9452−9462

Figure 4 shows a schematic diagram of the system with curved solid–liquid interfaces and contact angles of zero. The

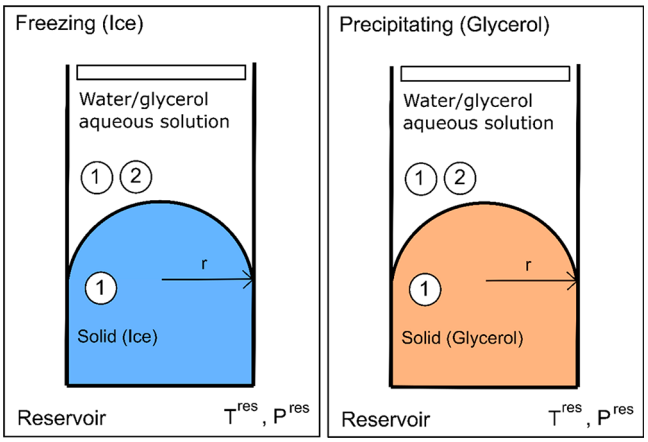

Figure 4. Schematic diagram of equilibrium with a curved solid–liquid interface and contact angle of zero. The freezing process is shown in the left panel, and the precipitating process is shown in the right panel.

left figure refers to the freezing process, and the right figure refers to the precipitating process. Component 1 represents the molecules that are present in both solid and liquid. Therefore, in the freezing process, component 1 is water and component 2 is glycerol. For the precipitating process, component 1 represents glycerol and component 2 represents water. According to the Gibbs Surface of Tension approach[4] that we have adopted, the solid–liquid interfacial tension is independent of curvature.

For all of the preceding equations, we have used the index 1 for the component that exists in both solid and liquid phases. Thus, for the left liquidus line (freezing of water as the solid), component 1 refers to water molecules, and all of the properties of water must be inserted into eq 41 or 42. For the right liquidus line (precipitating of glycerol as the solid), component 1 represents glycerol molecules, and all of the properties of glycerol must be inserted into eq 41 or 42. The properties of pure water and pure glycerol are tabulated in Table 1.

Table 1. Properties of Pure Water and Pure Glycerol at P^L = 1 atm[a]

	$T_{m,1}$ (K)	ΔH_1^{fus} (J/mol) at $T_{m,1}$	v_1^S (m^3/mol) at $T_{m,1}$
water	273.15	6010	1.963×10^{-5}
glycerol	291.35	18300	6.896×10^{-5}

[a]Data from ref 45.

2.3. Activity Coefficient Model. Equation 41 must be used along with a model to express the activity coefficient of component 1 (γ_1^L in eq 41). In this paper, we consider a solution consisting of water and glycerol. To model the activity coefficients, we used the Margules model and obtained the coefficients by fitting the model to solid–liquid equilibrium data for the water/glycerol system. For the water/glycerol system, the two-parameter Margules model gives a better fit compared to the osmotic virial equation.[46] γ_1^L is the activity coefficient of component 1, the component that is in both solid and liquid. To show the activity coefficients of different molecules clearly, here we use γ_w^L and γ_g^L to represent the activity coefficients of water and glycerol, respectively. x_w^L is the mole fraction of water in the liquid, and x_g^L is the mole fraction of glycerol. According to the general Margules equation, the activity coefficients of the two components of a binary system are given by

$$\ln(\gamma_w^L) = b_w(x_g^L)^2 + c_w(x_g^L)^3 + \ldots \quad (44)$$

$$\ln(\gamma_g^L) = b_g(x_w^L)^2 + c_g(x_w^L)^3 + \ldots \quad (45)$$

where coefficients b_g, c_g, ... are not independent and are related to b_w, c_w, ... through the Gibbs–Duhem equation at constant temperature and pressure. γ_1^L should be replaced by γ_w^L from eq 44 for the freezing process, and γ_1^L should be replaced by γ_g^L from eq 45 for the precipitating process. Considering the dependency of the coefficients (through the Gibbs–Duhem equation) and truncating the polynomials to third-order terms results in the two-parameter Margules equation[47]

$$\ln(\gamma_w^L) = [A_{wg} + 2(A_{gw} - A_{wg})x_w^L](x_g^L)^2 \quad (46)$$

$$\ln(\gamma_g^L) = [A_{gw} + 2(A_{wg} - A_{gw})x_g^L](x_w^L)^2 \quad (47)$$

Parameters A_{wg} and A_{gw} are obtained by fitting eq 41 in the absence of curvature ($r \to \infty$) along with eq 46 for the freezing process or along with eq 47 for the precipitating process to the experimental data of temperature versus the mole fraction of the left and right liquidus by minimizing the residual sum of squared errors. The Margules coefficients A_{wg} and A_{wg} are considered to be independent of temperature.

3. RESULTS AND DISCUSSION

3.1. Margules Coefficients for the Water/Glycerol System from Experimental Data. Figure 5 shows our fit

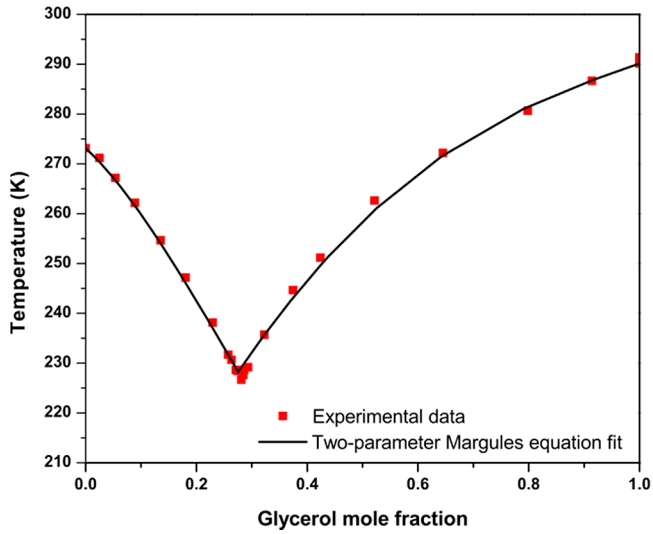

Figure 5. Fitting of the two-parameter Margules equation to the experimental solid–liquid equilibrium data for the water/glycerol system at P^L = 1 atm. Experimental data are from the work of Lane.[48]

of the two-parameter Margules equation to the experimental solid–liquid equilibrium data of Lane[48] for the water/glycerol binary system. Margules coefficients that minimize the residual sum of squared errors are presented in Table 2, along with the coefficient of determination (R^2). Because the two-parameter Margules equation fits the experimental data with a coefficient

DOI: 10.1021/acs.jpcb.7b07271
J. Phys. Chem. B 2017, 121, 9452–9462

Table 2. Parameters Obtained from Fitting the Two-Parameter Margules Model to the Experimental Data of Lane[48] at P^L = 1 atm

A_{wg}	A_{wg}	coefficient of determination, R^2
−1.0952	−2.1641	0.997

of determination close to 1, we conclude that the two-parameter Margules model adequately represents this data for our purposes.

3.2. Effect of Curvature on the Solid−Liquid Equilibrium Phase Diagram and the Eutectic Point for the Water/Glycerol System. Equation 41 gives the relationship between equilibrium temperature (T) and liquid mole fraction of the solidifying component (x_1^L). Values for the parameters $T_{m,1}$, ΔH_1^{fus}, and v_1^S can be found in Table 1. The activity coefficients of component 1 can be calculated from eq 46 or 47 with the parameters of the two-parameter Margules model shown in Table 2.

The interfacial tension is dependent on temperature and concentration,[49] but it is hard to measure the interfacial tension of a nanoscale solid particle with liquid directly by experiment.[50] It should be noted that the main goal of this article is to investigate the effect of curvature on the freezing and precipitating liquidus lines and on the eutectic point. Knowing the exact value of the interfacial tension would allow quantitative prediction of the equilibrium temperatures for the freezing and precipitating processes; however, the value is subject to change with the system's conditions. For simplicity, we assumed that the interfacial tension is constant and independent of temperature and concentration. We investigate the curvature effect at constant capillary radius r using 32 mN/m[51] as the interfacial tension of the ice−aqueous solution interfacial tension. There is a lack of experimental data and theoretical models for interfacial tension of glycerol precipitate with glycerol aqueous solution. Therefore, we make computations over a range of possible solid glycerol−aqueous solution interfacial tensions (100, 32, 10, and 1 mN/m). Figure 6 shows the temperature of equilibrium as a function of concentration where the radius of the capillary changes from 1 μm to 100, 10, and 5 nm for various possible values of interfacial tension.

According to Figure 6a,b, when the radius of the capillary is 1 μm or 100 nm, the freezing point and the solubility limit are not appreciably different from those of the flat surface. When the radius of the capillary decreases down to 10 nm, as shown

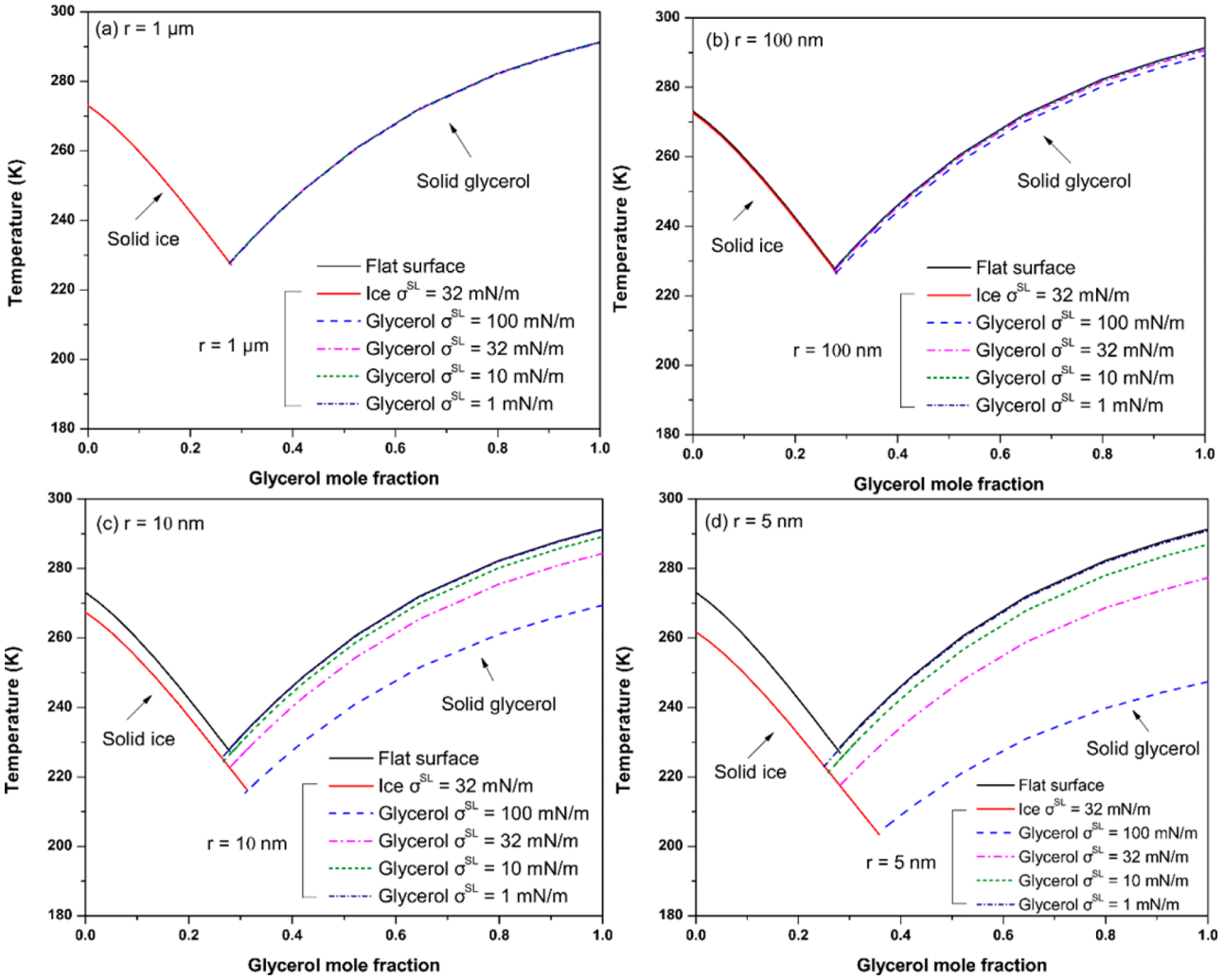

Figure 6. Predicted solid−liquid equilibrium phase diagram for the binary system of water and glycerol in capillaries at P^L = 1 atm with radii of (a) 1 μm, (b) 100 nm, (c)10 nm, and (d) 5 nm. Predictions are done over a range of possible glycerol solid−liquid interfacial tension values for lack of data to do precise calculation.

DOI: 10.1021/acs.jpcb.7b07271
J. Phys. Chem. B 2017, 121, 9452−9462

in Figure 6c, the freezing point is significantly decreased, and the decrease becomes larger when the capillary radius is reduced further down to 5 nm, as shown in Figure 6d.

The freezing point line (left-hand liquidus) and the precipitating line (right-hand liquidus) meet at the eutectic point. The eutectic point can be found by solving eq 43 together with eq 41 to see how the eutectic point temperature and concentration change with curvature. Figures 7 and 8

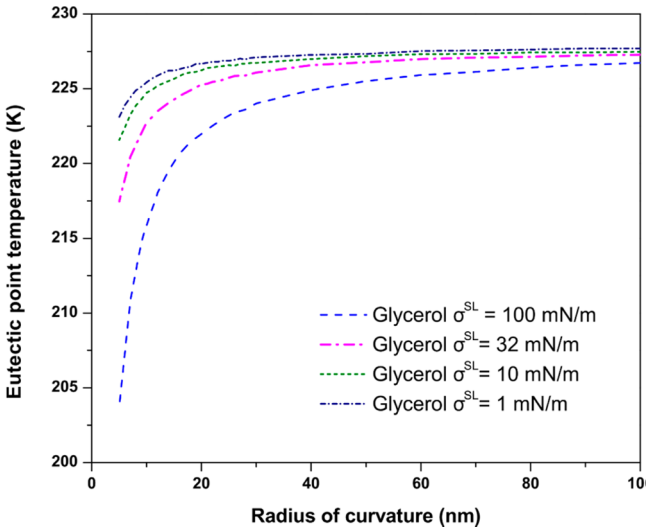

Figure 7. Predicted eutectic point temperature as a function of radius of curvature at P^L = 1 atm. Predictions are done over a range of possible glycerol solid−liquid interfacial tensions for lack of data to do a precise calculation.

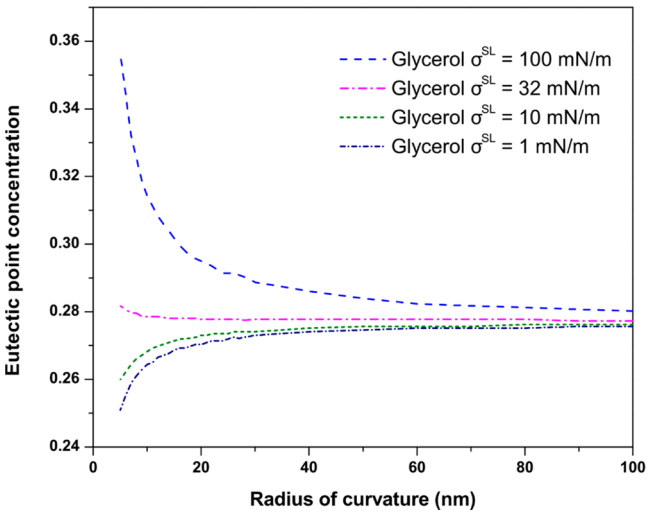

Figure 8. Predicted eutectic point concentration as a function of the radius of curvature at P^L = 1 atm. Predictions are done over a range of possible glycerol solid−liquid interfacial tensions for lack of data to do a precise calculation.

predict the eutectic point temperature and concentration as a function of radius of curvature in the range from 5 to 100 nm. Figure 7 shows how the eutectic point temperature changes with the radius of curvature. The eutectic point temperature of the water/glycerol system decreases as the radius of the capillary decreases. When the radius of curvature is around hundreds of nanometers, the eutectic point does not change appreciably as a function of the curvature. When the radius of curvature is under 100 nm, the eutectic point temperature has a significant drop from its flat interface value.

Figure 8 shows that the eutectic point concentration changes as a function of radius of curvature. The eutectic point concentration stays almost the same when the radius of curvature is above 100 nm. When the radius of curvature is less than 100 nm, the trend of the eutectic point concentration change depends on the difference between the solid glycerol−liquid interfacial tension and solid ice−liquid interfacial tension. If the glycerol σ^{SL} is bigger than the ice σ^{SL}, then the precipitating liquidus changes more than the freezing liquidus, which makes the eutectic point concentration increase as the radius of curvature decreases. If the glycerol σ^{SL} is smaller than the ice σ^{SL}, then the freezing liquidus changes more than the precipitating liquidus, which makes the eutectic point concentration decrease as the radius of curvature decreases. Regardless of the trend, the eutectic concentration changes significantly when the radius of curvature becomes less than 100 nm.

4. CONCLUSIONS

We have presented a derivation of thermal, mechanical, and chemical equilibrium conditions for solid−liquid equilibrium in a capillary of radius r, with different contact angles. We investigated the effect of curvature on solid−liquid equilibrium for the water/glycerol system. Curvature affects both the freezing process and the precipitating process. The solidifying points and the eutectic point temperature decrease as the radius of the capillary decreases, and when the radius of curvature is reduced to the nanoscale, the decrease becomes significant. The derived conditions for equilibrium shown for solid−liquid equilibrium can be applied to other multicomponent systems in capillary pores. The calculation procedure presented for a multicomponent phase diagram with curvature provides a way of combining chemical potential equilibrium with the mechanical equilibrium of a curved solid−liquid interface.

There are limitations to this work that can be enumerated and discussed: (1) The Margules parameters are considered to be independent of temperature. (2) The interfacial tensions between each solid and the aqueous liquid solution were taken to be constants, independent of curvature, concentration, and temperature. The shift of freezing point and eutectic point could be made accurately using the methods presented in this work if the glycerol solid−liquid interfacial tension were known. (3) Our calculations are based on the assumption that both ice−liquid and glycerol precipitate−liquid interfaces make a zero contact angle with the capillary solid wall.

This study gives a promising theoretical method to predict thermodynamic properties of solid−liquid equilibrium across a curved interface in nonideal multicomponent systems (demonstrated here for a binary system but extendable to multicomponent cases) that has applications in many fields such as cryobiology, forestry, and soil sciences. In cryobiology, the freezing point of solutions containing diverse solutes, including salts, cryoprotectants, proteins, and many other macromolecules in confined spaces such as membrane pores, is of vital importance.[18−20,41,44] Furthermore, during freezing, direct cell injury has been associated with eutectic crystallization.[52] In forestry, in the xylem parenchyma of hardwood tree species and in dormant flower bud primordia of woody species, extracellular water exists in microcapillaries in the extracellular space.[18] These microcapillaries can depress the freezing point of water in the intercellular spaces and impede

DOI: 10.1021/acs.jpcb.7b07271
J. Phys. Chem. B 2017, 121, 9452−9462

the spread of ice through the tissue. The freezing point depression of the microcapillaries can help the plant survive at low temperature. In soil science, the freezing and melting of water in porous particles that are abundant in soil are of critical interest in cold regions because of their role in frost damage. Previously, solid−liquid equilibrium inside porous media has been studied for ice with pure water.[53,54] With our equations, the prediction of freezing and melting temperatures in nanoscale pores in soil could be extended to water that contains various soluble substances, such as salt or organic components that are abundant in soil.

AUTHOR INFORMATION

Corresponding Author

*E-mail: janet.elliott@ualberta.ca.

ORCID

Hyun-Joong Chung: 0000-0003-0569-6951

Janet A. W. Elliott: 0000-0002-7883-3243

Notes

The authors declare no competing financial interest.

ACKNOWLEDGMENTS

This research was funded by the Natural Sciences and Engineering Research Council (NSERC) of Canada. J.A.W.E. holds a Canada Research Chair in Thermodynamics.

REFERENCES

(1) Thomson, S. W. On the Equilibrium of Vapour at a Curved Surface of Liquid. *Proc. R. Soc. Edinburgh* **1872**, *7*, 63−68.

(2) Elliott, J. A. W. On the Complete Kelvin Equation. *Chem. Eng. Educ.* **2001**, *35*, 274−278.

(3) Melrose, J. C. Model Calculations for Capillary Condensation. *AIChE J.* **1966**, *12* (5), 986−994.

(4) (a) Gibbs, J. W. On the Equilibrium of Heterogeneous Substances, in *Transactions of the Connecticut Academy of Arts and Sciences*, Vol. 3, 1874−1878, pp 108−248 and 343−524. DOI: 10.11588/heidok.00013220. (b) Gibbs, J. W. *The Scientific Papers of J. Willard Gibbs*, Ox Bow: Woodbridge, CT, 1993, Vol I., pp 5−353.

(5) Fisher, L. R.; Israelachvili, J. N. Direct Experimental Verification of the Kelvin Equation for Capillary Condensation. *Nature* **1979**, *277*, 548−549.

(6) Fisher, L. R.; Israelachvili, J. N. Experimental Studies on the Applicability of the Kelvin Equation to Highly Curved Concave Menisci. *J. Colloid Interface Sci.* **1981**, *80* (2), 528−541.

(7) Shapiro, A. A.; Stenby, E. H. Kelvin Equation for a Non-Ideal Multicomponent Mixture. *Fluid Phase Equilib.* **1997**, *134*, 87−101.

(8) Ward, C. A.; Balakrishnan, A.; Hooper, F. C. On the Thermodynamics of Nucleation in Weak Gas−Liquid Solutions. *J. Basic Eng.* **1970**, *92* (10), 695−704.

(9) Shapiro, A. A.; Stenby, E. H. Thermodynamics of the Multicomponent Vapor−Liquid Equilibrium under Capillary Pressure Difference. *Fluid Phase Equilib.* **2001**, *178* (1), 17−32.

(10) Eslami, F.; Elliott, J. A. W. Design of Microdrop Concentrating Processes. *J. Phys. Chem. B* **2013**, *117* (7), 2205−2214.

(11) Eslami, F.; Elliott, J. A. W. Stability Analysis of Microdrops During Concentrating Processes. *J. Phys. Chem. B* **2014**, *118* (13), 3630−3641.

(12) Webber, J. B. W. Studies of Nano-Structured Liquids in Confined Geometries and at Surfaces. *Prog. Nucl. Magn. Reson. Spectrosc.* **2010**, *56* (1), 78−93.

(13) Liu, Z.; Muldrew, K.; Wan, R. G.; Elliott, J. A. W. Measurement of Freezing Point Depression of Water in Glass Capillaries and the Associated Ice Front Shape. *Phys. Rev. E* **2003**, *67*, 61602.

(14) Christenson, H. K. Confinement Effects on Freezing and Melting. *J. Phys.: Condens. Matter* **2001**, *13*, R95−R133.

(15) Findenegg, G. H.; Jähnert, S.; Akcakayiran, D.; Schreiber, A. Freezing and Melting of Water Confined in Silica Nanopores. *ChemPhysChem* **2008**, *9* (18), 2651−2659.

(16) Fagerlund, G. Determination of Pore-Size Distribution from Freezing-Point Depression. *Mater. Constr.* **1973**, *6* (3), 215−225.

(17) Hirama, Y.; Takahashi, T.; Hino, M.; Sato, T. Studies of Water Adsorbed in Porous Vycor Glass. *J. Colloid Interface Sci.* **1996**, *184* (2), 349−359.

(18) Ashworth, E. N.; Abeles, F. B. Freezing Behavior of Water in Small Pores and the Possible Role in the Freezing of Plant Tissues. *Plant Physiol.* **1984**, *76* (1), 201−204.

(19) Mazur, P. The Role of Cell Membranes in the Freezing of Yeast and Other Single Cells. *Ann. N. Y. Acad. Sci.* **1965**, *125*, 658−676.

(20) Acker, J. P.; Elliott, J. A. W.; McGann, L. E. Intercellular Ice Propagation: Experimental Evidence for Ice Growth Through Membrane Pores. *Biophys. J.* **2001**, *81*, 1389−1397.

(21) Jacot, A.; Rappaz, M. A Pseudo-Front Tracking Technique for the Modelling of Solidi Cation Microstructures in Multi-Component Alloys. *Acta Mater.* **2002**, *50*, 1909−1926.

(22) Ostwald, W. On the Assumed Isomerism of Red and Yellow Mercury Oxide and the Surface-Tension of Solid Bodies. *Z. Phys. Chem.* **1900**, *34*, 495.

(23) Freundlich, H. Kapillarchemie. *Akademische Verlagsgesellschaft* **1922**.

(24) Defay, R. *Surface Tension and Adsorption*, English ed.; Longmans: London, England, 1966.

(25) Freundlich, H. *Colloid and Capillary Chemistry*; E. P. Dutton and Company: New York, 1923.

(26) Eslami, F.; Elliott, J. A. W. Role of Precipitating Solute Curvature on Microdrops and Nanodrops during Concentrating Processes: The Nonideal Ostwald−Freundlich Equation. *J. Phys. Chem. B* **2014**, *118*, 14675−14686.

(27) Tan, S. P.; Piri, M. Equation-of-State Modeling of Associating-Fluids Phase Equilibria in Nanopores. *Fluid Phase Equilib.* **2015**, *405*, 157−166.

(28) Shardt, N.; Elliott, J. A. W. Thermodynamic Study of the Role of Interface Curvature on Multicomponent Vapor−Liquid Phase Equilibrium. *J. Phys. Chem. A* **2016**, *120* (14), 2194−2200.

(29) Tan, S. P.; Piri, M. Equation-of-State Modeling of Confined-Fluid Phase Equilibria in Nanopores. *Fluid Phase Equilib.* **2015**, *393*, 48−63.

(30) Tanaka, T.; Hara, S.; Cermak. Thermodynamic Evaluation of Binary Phase Diagram of Small Particle Systems. *Z. Metallkd.* **2001**, *92*, 467−472.

(31) Jesser, W. A.; Shneck, R. Z.; Gile, W. W. Solid−Liquid Equilibria in Nanoparticles of Pb-Bi Alloys. *Phys. Rev. B* **2004**, *69* (14), 1−13.

(32) Seiler, M.; Groß, J.; Bungert, B.; Sadowski, G.; Arlt, W. Modeling of Solid/Fluid Phase Equilibria in Multicomponent Systems at High Pressure. *Chem. Eng. Technol.* **2001**, *24* (6), 607−612.

(33) Walas, S. M. *Phase Equilibria in Chemical Engineering*; Butterworth: Boston, MA, 1985.

(34) Miner, C.; Dalton, N. Glycerine: An Overview. *Chem. Soc. Monogr.* **1953**, *117* (212), 1−27.

(35) Polge, C.; Smith, A. U.; Parkes, A. S. Revival of Spermatozoa after Vitrification and Dehydration at Low Temperatures. *Nature* **1949**, *164*, 666.

(36) Callen, H. B. *Thermodynamics and an Introduction to Thermostatistics*, 2nd Ed., John Wiley & Sons: New York, 1985.

(37) Polyanin, A. D; Manzhirov, A. V. *Handbook of Mathematics for Engineers and Scientists*; CRC Press, 2006.

(38) Elliott, J. A. W.; Prickett, R. C.; Elmoazzen, H. Y.; Porter, K. R.; McGann, L. E. A Multisolute Osmotic Virial Equation for Solutions of Interest in Biology. *J. Phys. Chem. B* **2007**, *111*, 1775−1785.

(39) Prickett, R. C.; Elliott, J. A. W.; McGann, L. E. Application of the Osmotic Virial Equation in Cryobiology. *Cryobiology* **2010**, *60* (1), 30−42.

(40) Elliott, J. R.; Lira, C. T. *Introductory Chemical Engineering Thermodynamics*; Prentice-Hall Inc: Upper Saddle River, NJ, 2012; pp 450.

DOI: 10.1021/acs.jpcb.7b07271
J. Phys. Chem. B 2017, 121, 9452−9462

(41) Zielinski, M. W.; McGann, L. E.; Nychka, J. A.; Elliott, J. A. W. Comparison of Non-Ideal Solution Theories for Multi-Solute Solutions in Cryobiology and Tabulation of Required Coefficients. *Cryobiology* **2014**, *69*, 305−317.
(42) Du, Y. J.; Yen, T. T.; Chen, L. R. Theoretical Calculation of the Mole Fraction at the Eutectic Point for a Binary System. *Phys. Status Solidi B* **1985**, *130* (1), K5−K10.
(43) Olawale, M.; Amuda, H.; Akabekwa, R. O. Estimating the Eutectic Composition of Simple Binary Alloy System Using Linear Geometry. *Leonardo J. Sci.* **2008**, *12*, 232−242.
(44) Htira, T.; Cogné, C.; Gagnière, E.; Mangin, D. Determination of the Solid−Liquid Phase Diagram of the Binary System Propionic Acid/Water. *J. Chem. Eng. Data* **2016**, *61* (2), 806−812.
(45) *CRC Handbook of Chemistry and Physics*; Knovel: Binghamton, NY, 2017.
(46) Zargarzadeh, L.; Elliott, J. A. W. Comparison of the Osmotic Virial Equation with the Margules Activity Model and Their Application to Solid−Liquid Equilibrium. **2017**, to be submitted.
(47) Prausnitz, J. M.; Lichtenthaler, R. N.; Azevedo, E. G. d. *Molecular Thermodynamics of Fluid-Phase Equilibria*, 3rd ed.; Pearson Education, 1998.
(48) Lane, L. B. Freezing Points of Glycerol and Its Aqueous Solutions. *Ind. Eng. Chem.* **1925**, *17*, 924.
(49) Takamura, K.; Fischer, H.; Morrow, N. R. Physical Properties of Aqueous Glycerol Solutions. *J. Pet. Sci. Eng.* **2012**, *98*−*99*, 50−60.
(50) Binks, B. P.; Clint, J. H. Solid Wettability from Surface Energy Components: Relevance to Pickering Emulsions. *Langmuir* **2002**, *18* (4), 1270−1273.
(51) Hillig, W. B. Measurement of Interfacial Free Energy for Ice/Water System. *J. Cryst. Growth* **1998**, *183* (3), 463−468.
(52) Han, B.; Bischof, J. C. Direct Cell Injury Associated with Eutectic Crystallization During Freezing. *Cryobiology* **2004**, *48* (1), 8−21.
(53) Peppin, S. S. L.; Style, R. W. The Physics of Frost Heave and Ice-Lens Growth. *Vadose Zone J.* **2013**, *12*, 1.
(54) Jackson, K. A.; Chalmers, B. Freezing of Liquids in Porous Media with Special Reference to Frost Heave in Soils. *J. Appl. Phys.* **1958**, *29* (8), 1178−1181.

DOI: 10.1021/acs.jpcb.7b07271
J. Phys. Chem. B 2017, 121, 9452−9462